https://doi.org/10.5194/egusphere-2025-4429
Preprint. Discussion started: 26 September 2025

Intraseasonal modulation of Sea Surface Temperatures in the North Tropical Atlantic by African Easterly Waves

Marc K. Mendy [1,2], Florent Gasparin [2], Manon Gévaudan [3], Moussa Diakhaté [2], Issa Sakho [2], Julien Jouanno [1]

[1] Université de Toulouse, LEGOS (IRD/UT3/CNES/CNRS), Toulouse, France,
[2] Université Amadou Mahtar Mbow, Diamniadio, Sénégal,
[3] Centre National de Recherches Météorologiques, CNRM-CNRS, Météo-France, Toulouse, France

Correspondance to: Marc K. Mendy (marckakantemendy@gmail.com)

Abstract. The sea surface temperature (SST) variability in the North Tropical Atlantic plays a crucial role in the regional climate by modulating the Intertropical Convergence Zone (ITCZ) and influencing precipitation, convective systems, and tropical cyclones. While atmospheric synoptic-scale intraseasonal variability in this region is dominated by African Easterly Waves (AEWs), their impact on SST remains poorly understood. This study investigates the modulation of SST by AEWs using a regional configuration of a coupled ocean-atmosphere model and PIRATA mooring air-sea observations. Results reveal a significant AEWs signature in SST anomalies, with temperature fluctuations exceeding ±0.5°C. A heat budget analysis shows that AEWs mainly influence SST through modulation of the latent heat flux, shortwave radiation, and vertical mixing. The contribution of the ocean mixing and that of the air-sea fluxes appear of similar order, likely reflecting the influence of near-inertial currents. The dominant 3–5-day AEWs exhibit a stronger impact than their 6–9-day counterparts. These findings highlight the role of AEWs in driving SST variability and mixed-layer dynamics, underscore the importance of accurately representing them in coupled climate models, and call for further investigation into their influence on the mean and seasonal upper-ocean state.

Key points:

1. A regional coupled ocean-atmosphere model accurately simulates AEWs ocean response.
2. SST response is controlled by both vertical mixing and air-sea fluxes
3. 3–5-day AEWs exhibit a stronger impact on SST than 6–9-day AEWs

https://doi.org/10.5194/egusphere-2025-4429
Preprint. Discussion started: 26 September 2025

1 Introduction

The variability of the sea surface temperature (SST) in the North Tropical Atlantic is a key factor in determining the regional climate and affects surrounding countries. It plays a critical role in modulating the position of the Intertropical Convergence Zone (ITCZ) (Wane et al., 2021), as shown by the strong correlation between the ITCZ and the regions of highest SST (zonal band of SST ≥ 27°C) (Graham and Barnett, 1987; Waliser and Graham, 1993; Opoku-Ankomah and Cordery, 1994). This variability plays a key role in establishing and maintaining convective systems and precipitation in the tropical Atlantic, West Africa, and northeastern South America (Moura and Shukla, 1981; Hastenrath and Greischar, 1993; Nobre and Shukla, 1996; Sultan and Janicot, 2000; Nicholson, 2009; Tomaziello et al., 2016). Furthermore, the frequency and intensity of tropical cyclones, which draw their energy from the warm waters of the Tropical Atlantic, are influenced by these SST anomalies (Emanuel, 2005; Webster et al., 2005). Therefore, a better understanding of the mechanisms involved in SST variability is essential not only to enhance our comprehension of climate processes, but also to reduce SST biases in coupled models and refine climate forecasts.

At the synoptic scale, atmospheric variability in this region is predominantly governed by African Easterly Waves (AEWs) (Thompson et al., 1979; Diedhiou et al., 2001). These are eastward-propagating atmospheric disturbances with periods ranging from 2 to 10 days, which develop during the boreal summer over the tropical region, primarily across West Africa. AEWs generally originate from atmospheric instabilities, particularly barotropic-baroclinic instabilities associated with the African Easterly Jet (Burpee, 1972). They also originate from convection, which not only facilitates their initiation but can also enhance their growth (Berry and Thorncroft, 2005; Mekonnen et al., 2006; Thorncroft et al., 2008; Russell et al., 2020). AEWs are generally classified into two period bands: 3-5 days and 6-9 days (Diedhiou et al., 1998a, b, 1999; Felice et al., 1990, 1993; Wu et al., 2013). The 3-5 days AEWs propagate preferentially on either side of the African Easterly Jet, before merging over the Atlantic, generally at around 17.5°N. They have average wavelengths of around 3,000 km and phase speeds of up to 10 m/s (Diedhiou et al., 1998a; Reed et al., 1988; Thorncroft and Hodges, 2001). Those of 6 to 9 days, further north and more intermittent, unfold with an average phase speed of around 6 m/s and wavelengths of around 5000 km (Diedhiou et al., 2010; Wu et al., 2013).

On their trajectory, AEWs interact closely with deep convection, playing a central role in modulating atmospheric dynamics in West Africa. Several studies have highlighted the influence of AEWs on the organization, intensity and propagation of mesoscale convective systems (Berry and Thorncroft, 2005; Kiladis et al., 2006; Russell et al., 2020). In particular, these interactions are manifested by an amplification of convection in cyclonic convergence zones associated with wave troughs, thus promoting the triggering or intensification of precipitation (Fink and Reiner, 2003; Kiladis et al., 2006). Moreover, under certain favorable conditions, particularly when deep convection persists downstream of the wave, these systems can contribute to the cyclogenesis process in the North Tropical Atlantic

https://doi.org/10.5194/egusphere-2025-4429
Preprint. Discussion started: 26 September 2025

(Thorncroft and Hodges, 2001; Dunkerton et al., 2009; Russell et al., 2017; Bercos-Hickey and Patricola, 2025).

In the North Tropical Pacific, Mickett et al. (2010), using a slab model and comparing surface wind-induced inertial kinetic energy fluxes in the mixed layer, show that these waves (Pacific Easterly Waves, PEWs) resonantly force inertial motions, which influence sea surface temperatures. In their recent work, Hummels et al. (2020) put forward the hypothesis that, in the North Tropical Atlantic, AEWs would contribute to cooling the ocean surface, through the associated latent heat fluxes, and the strong vertical mixing at the base of the mixed layer induced by the quasi-inertial waves they would generate. However, their importance in the regional heat balance, and consequently on surface temperature, remains to be clarified. While numerous studies have investigated the characteristics of AEWs and their role in climate modulation, to our knowledge no study has yet examined their impact on ocean surface conditions in the Tropical Atlantic. Using a coupled ocean–atmosphere configuration of the Tropical Atlantic (Gévaudan et al., 2021), the aim of this study is to examine whether AEWs influence SST in this region and investigate the underlying mechanisms.

The paper is organized as follows: the Tropical Atlantic coupled model and the validation datasets are presented in Section 2. A comparison of model and observations SST and winds associated with AEWs is provided in Section 3. Section 4 examines the ocean surface response to AEWs by projecting a representative AEWs index, derived from near-surface winds, onto SST. Section 5 investigates the underlying mechanisms based on the analysis of the ocean heat balance in the surface layer. Finally, the conclusion and perspectives are provided in Section 6.

2 Data and methodological approach

2.1 Regional coupled model

This study is based on a regional configuration of the coupled NEMO-WRF model sharing the same horizontal grid at a resolution of ¼° (~ 27 km) for the tropical Atlantic (99°W-20°E, 15°S-35°N) (Gévaudan et al., 2021, 2022). These two models interact on an hourly basis, exchanging SST, surface currents, surface stress, air-heat surface fluxes and freshwater fluxes via the OASIS coupler. The parameterization follows that of Gévaudan et al. (2021), with updates to align it with more recent versions of the various codes: NEMO-v4.2.1 (Madec et al., 2023) and WRF-v4.2.1 (Skamarock et al., 2019). The models are coupled using OASIS3-MCT V4.0 (Valcke and Redler, 2012; Craig et al., 2017).

The ocean model solves the three-dimensional primitive equations, has 75 fixed vertical levels (z coordinates), with 12 levels in the upper 20 m and 24 levels in the upper 100 m. Lateral open boundaries of the model are prescribed using an interannual hindcast of temperature, salinity, sea level and horizontal velocities from the MERCATOR global daily reanalysis GLORYS2V4 (Ferry et al., 2012). To include ocean color in the solar radiation penetration scheme, the model is driven by daily

https://doi.org/10.5194/egusphere-2025-4429
Preprint. Discussion started: 26 September 2025

chlorophyll concentrations from GlobColour 009_082, derived from several satellite products (Maritorena et al., 2010; Garnesson et al., 2019). The atmospheric model WRF solves the compressible, non-hydrostatic Euler equations using the Advanced Research WRF (ARW) dynamical solver. It employs a grid with 40 terrain-following vertical levels (sigma coordinates), with the top of the atmosphere set at 50 hPa. Lateral boundary conditions are given by 3-hourly atmospheric fields from the ERA5 reanalysis from the European Centre for Medium-Range Weather Forecasts (ECMWF) (Hersbach et al., 2020).

The ocean model was initialized on January 1, 2000, based on a forced NEMO simulation of 20 years (1980-1999). The atmospheric model was initialized from ERA5 reanalysis on January 1, 2000. The coupled model is spun up for one year (2000), then run over a 21-year period (2001–2021), producing daily outputs of oceanic and atmospheric fields. To investigate the processes that drive the SST variations associated with AEWs, the different contributions to the 3D temperature balance are computed online at each grid point and saved daily (details are given in Section 5).

2.2 Validation datasets

To validate the simulations, a variety of datasets covering the period from 2001 to 2021 were used. These include the ERA5 reanalysis, which uses advanced modelling and data assimilation systems to combine vast amounts of historical observations with global estimates (Hersbach et al., 2020). For this study, the 10-m surface winds (u10 and v10), the winds along the atmospheric column (u and v) and the daily available SST at 1/4° were used to validate the performance of our model in reproducing the dynamics and thermodynamics in our study area. In addition, winds measured by the Advanced SCATterometer (ASCAT), which is on board the operational meteorological satellite MetOp, are used. These data are available on a 1/4° horizontal grid with a daily time step since 2007 (J. Figa-Saldaña and Stoffelen, 2002).

The model's SST is also compared to NOAA's Optimum Interpolation Sea Surface Temperature (OISST) version 2.0, which is a combination of satellite observations (AVHRR), in-situ measurements from ships and buoys, adjusted to fill gaps by optimal interpolation (Reynolds et al., 2007; Banzon et al., 2016). These data are available at 1/4° resolution and daily frequency from late 1981 to the present and are representative of skin SSTs. Finally, daily wind at 4 m and surface temperature at 1 m derived from the entire PIRATA mooring array (Bourlès et al., 2008) in the tropical North Atlantic were also used to validate the model. Note that these PIRATA buoy wind measurements taken at 4 m ($\mathrm{Wind}_{4\mathrm{m}}$) are scaled to 10-m wind speeds ($\mathrm{Wind}_{10\mathrm{m}}$) using a logarithmic wind profile for neutral conditions as $\mathrm{Wind}_{10\mathrm{m}} = \mathrm{Wind}_{4\mathrm{m}} \left(\frac{\ln(10\mathrm{m}/z_0)}{\ln(4\mathrm{m}/z_0)}\right)$, with z_0 the surface roughness length ($z_0 = 0.0002$) (Fleagle and Businger, 1981; Dutton, 1986).

https://doi.org/10.5194/egusphere-2025-4429
Preprint. Discussion started: 26 September 2025

2.3 Identification of AEWs

To identify AEWs, we apply a Butterworth band-pass filter to the time series, retaining variability in the 2–10-day period. This range is widely used in the literature as it encompasses the typical synoptic variability associated with AEWs (Russell et al., 2017; Danso et al., 2022; Jonville et al., 2025). This involves applying temporal filtering techniques (e.g., Butterworth or Lanczos filters) to the target variables to isolate the part associated with AEWs. Other approaches, such as spectral analysis (Wheeler and Kiladis, 1999; Fink and Reiner, 2003; Jiang et al., 2023) and Lagrangian tracking methods (Carlson, 1969; Thorncroft and Hodges, 2001) are also used to detect AEWs. These techniques make it possible to track the spatio-temporal evolution of AEWs troughs and identify their implications in modulating local climate. However, in the output fields of mesh models or reanalysis, temporal filtering remains a robust method for isolating AEWs signals over large domains (Skinner and Diffenbaugh, 2013; Jonville et al., 2024). We focus on the July–August–September (JAS) period, which is widely used in the literature to study AEWs (Janiga and Thorncroft, 2013; Bercos-Hickey et al., 2017; Semunegus et al., 2017; Raj et al., 2023), as it corresponds to the peak season of AEWs activity (Grist, 2002).

3 Evaluation of the coupled model

First, we assess the model's ability to reproduce AEWs and surface ocean conditions. To this end, we focus on both the mean state and the high-frequency variability of key variables: SST, surface wind at 10 m, and the vertical wind structure along 20°W.

3.1 Sea surface temperature

The mean SST and the standard deviation of SST anomalies filtered between 2 and 10 days are shown in Figure 1. Overall, the mean SST distribution is well reproduced by the model. In the western part of the basin, the Atlantic Warm Pool - defined as the area where SSTs exceed 28°C during boreal summer (Enfield and Lee, 2005; Wang et al., 2006, 2008) - extends slightly further east than the estimates from ERA5, OISST and PIRATA moorings. Off the African coast, between 21°N and 25°N, the model represents well the cool SSTs associated with the Moroccan upwelling system. Southeast of the Equator, the Atlantic cold tongue is characterized by SSTs around 24°C during the boreal summer, partly attributed to Ekman divergence induced by the southeast trade winds crossing the Equator (Cromwell, 1953; Stommel, 1959), and vertical turbulent mixing (Jouanno et al., 2011; Wade et al., 2011). Coupled models often underestimate this cooling, which could account for the slight temperature bias observed in the eastern tropical Atlantic (Fig. 1), a well-known issue in climate simulations (Shi et al., 2018; Voldoire et al., 2019; Deppenmeier et al., 2020).

https://doi.org/10.5194/egusphere-2025-4429
Preprint. Discussion started: 26 September 2025

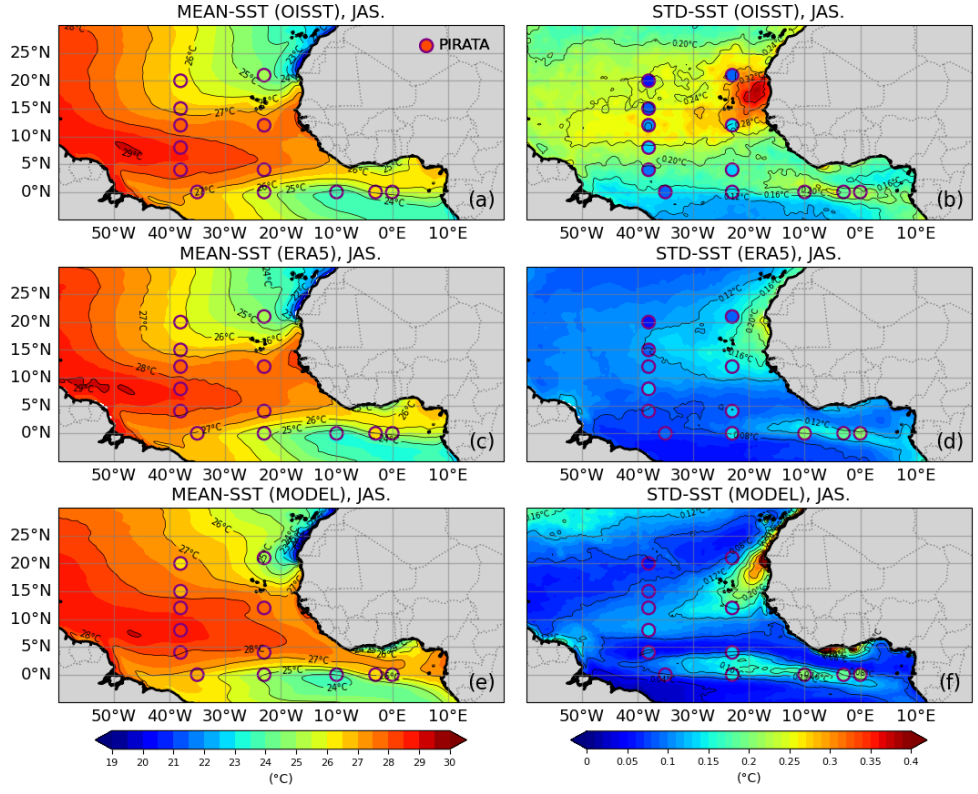

Figure 1: (Left panels) Mean SST, and (right panels) standard deviation of SST anomalies for July–August–September (JAS) over the 2007–2021 period, from (a), (b) OISST, (c), (d) ERA5, and (e), (f) the coupled model. The standard deviation is computed from anomalies band-pass filtered in the 2–10-day range. In each panel, estimates from the PIRATA mooring are indicated by circles.

The standard deviation of SST anomalies filtered in the 2–10-day band reveals substantial amplitude differences among the various products (Fig. 1bdf). A much larger variability is observed in OISST (Fig. 1b) than in the other data sources. The difference might be due to the distinct nature of these observations. Satellites measure the temperature of the ocean's uppermost micrometers, known as "skin temperature", whereas in situ sensors, such as those used by PIRATA, record the temperature averaged over approximately 1 m, referred to as "bulk temperature". The vertical resolution of our ocean model and the model used to force the ERA5 reanalysis are both around 1 m. This difference in depth makes skin temperature more sensitive to high-frequency variations, particularly those driven by atmospheric influences and changing weather conditions (Murray et al., 2000; Donlon et al., 2002) The patterns of high variability also differ between ERA5 and the model, and comparison with PIRATA moorings indicates that the coupled model performs better than ERA5 (Fig. 1df). Contrary to ERA5, the model accurately captures the two areas of enhanced variability: the zonal band along the northern front of the

https://doi.org/10.5194/egusphere-2025-4429
Preprint. Discussion started: 26 September 2025

Atlantic cold tongue (moorings between 0° and 5°N), and the band further north (between 10° and 20°N), oriented southwestward.

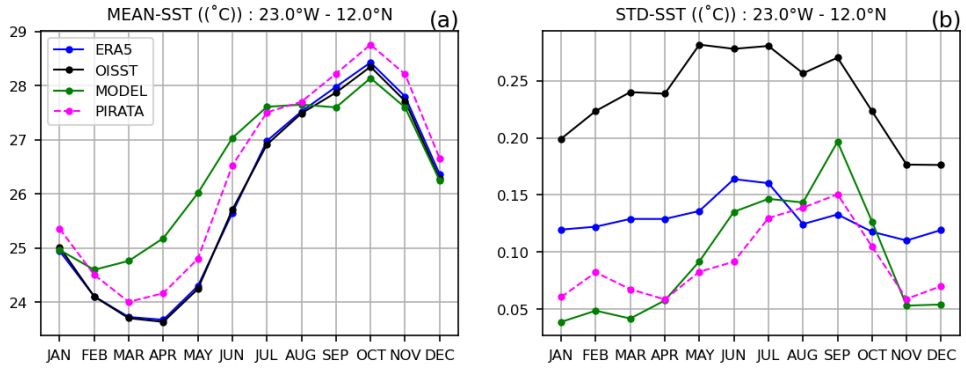

Figure 2: (a) Monthly climatology of SST, and (b) standard deviation of SST anomalies at 23°W–12°N over the 2001–2021 period of OISST (black), ERA5 (blue), the coupled model (green), and the 23°W-12°N PIRATA mooring (pink). Anomalies are band-pass filtered in the 2–10-day range prior to computing the standard deviation.

Figure 2 presents the SST climatology (from 2001 to 2021) and the standard deviation of SST anomalies filtered in the 2–10-day band for different datasets at 23°W-12°N. This point is the location of a PIRATA mooring that lies within a region of pronounced high-frequency SST variability (Fig. 1f). The seasonal cycle of SST is broadly consistent across the different estimates, with the model showing a warm bias of about 1°C compared to PIRATA from March to May, and smaller biases (<0.5°C) during the rest of the year—well below the typical biases found in climate coupled models for this region (Richter and Tokinaga, 2020). Differences are much larger regarding the high frequency SST variability, and reflect some of the differences already inferred in Fig. 1d-f. OISST shows nearly twice the variability of the other products, while ERA5 exhibits a flat seasonal cycle. This higher OISST variability could result from biases of satellite measurements that cannot be resolved by Huang et al. (2021) algorithms. This suggests that state-of-the-art products such as OISST and ERA5 may not be well-suited for investigating high-frequency SST variations in this region. Unlike OISST and ERA5, the model is in good agreement with PIRATA observations, and accurately captures the seasonal cycle of 2–10-day SST variability, reaching a maximum in July-September (Fig. 2b).

3.2 10-meter winds

We now assess the model's ability to reproduce surface wind conditions by comparing 10-m winds from the coupled model with those from ERA5, the ASCAT scatterometer, and in-situ PIRATA measurements. Figure 3 presents the mean 10-m wind (speed and direction) and the standard deviation of anomalies band-pass filtered in the 2–10-day range for the JAS period. On average, the different products show the convergence of the trade winds from the North-East and South-East towards the

https://doi.org/10.5194/egusphere-2025-4429
Preprint. Discussion started: 26 September 2025

region of maximum SST (here > 27°C, Fig. 1), which appears to be a response of the winds to the SST anomalies (Sweet et al., 1981; Wallace et al., 1989). This pattern defines the ITCZ, located west of 30°W and around 8°N at this time of year. The ITCZ then tilts northward (between 10°N and 15°N) on the east, following the SST maximum (Gill, 1980). In this region, after crossing the equator, the southern trade winds are deflected eastward by the effect of the Coriolis force. As these winds carry moisture, they bring the West African monsoon onto the continent during the summer. These characteristics are very well reproduced by the coupled model, despite a slight positive bias (< 0.5m/s) compared to ASCAT. ERA5, in turn, is closer to PIRATA and ASCAT along the position of the ITCZ and the West African coast, with a negative bias over the rest of the basin. Exhibiting a pattern similar to the 2–10-day SST variability (Fig. 1), the 10-m wind variability is pronounced along the West African coast and extends offshore. The highest variability occurs off the coasts of Senegal and Mauritania, with values reaching up to 2 m/s.

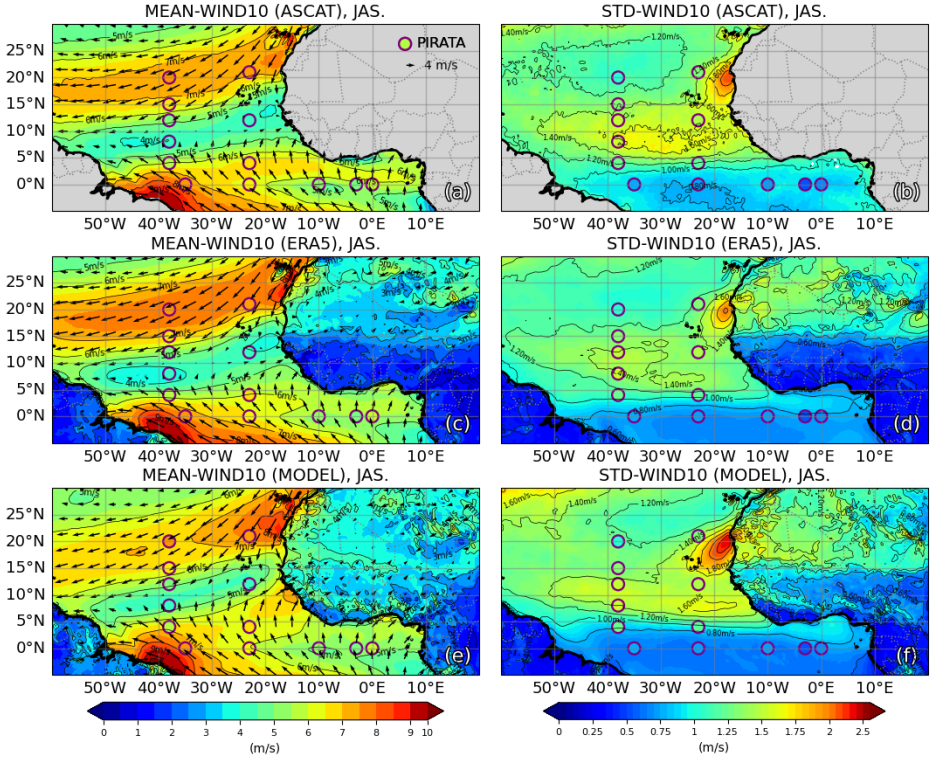

Figure 3: 10-m wind speed for the months of July-August-September (left panels) and corresponding standard deviation (right panels) over the 2001–2021 period for (a), (b) ASCAT, (c), (d) ERA5 and (e), (f) the coupled model. The standard deviation is computed from anomalies filtered in the 2–10-day band. In each panel, PIRATA mooring values are indicated by circles.

https://doi.org/10.5194/egusphere-2025-4429
Preprint. Discussion started: 26 September 2025

The monthly climatology of the 10-m wind and the corresponding standard deviation of anomalies in the 2–10-day frequency band are shown in Figure 4 for the model, ERA5, ASCAT and the PIRATA mooring at 23°W-12°N. A clear seasonality of the 10-m winds is seen, with minimum values in summer, corresponding to the passage of the ITCZ, and maximum values in winter. The different products exhibit similar seasonal fluctuations, with an overall average difference lower than 0.5 m/s. The 2–10-day variability of the wind at 10 m peaks in summer, with little difference between the model and the other products (< 0.2 m/s).

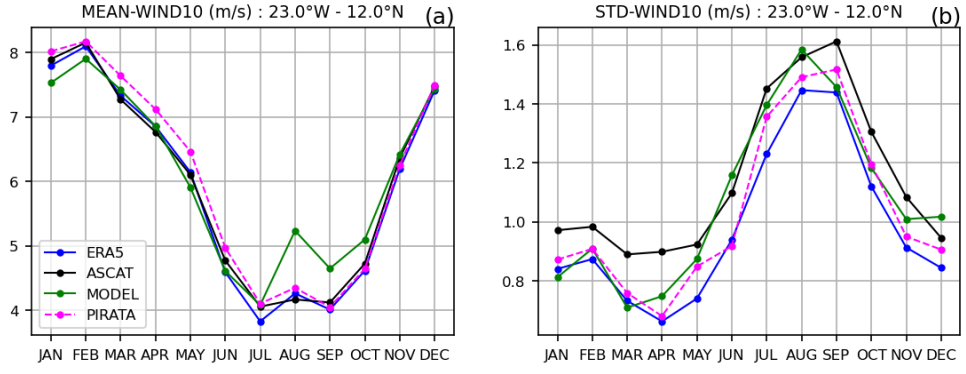

Figure 4: (a) Monthly climatology and (b) monthly standard deviation of the 10-m wind speed at 23°W–12°N over the 2001–2021 period for ASCAT (black), ERA5 (blue), the coupled model (green), and the 23°W-12°N PIRATA mooring. The standard deviation is computed from anomalies filtered in the 2–10-day band.

3.3 Vertical wind structure

In this region, wind variability on timescales of 2 to 10 days is largely driven by AEWs. However, this range is quite broad, and it is well known that there are actually two distinct regimes, which we will refer to as southern and northern AEWs, each characterized by different vertical structures, periods, and horizontal distributions (Diedhiou et al., 1998b, 1999; Felice et al., 1990; Viltard et al., 1997). The objective here is to assess whether the model can accurately capture both types of AEWs: those with periods of 3–5 days ($AEWs_{3-5day}$) and those with periods of 6–9 days ($AEWs_{6-9day}$).

Figure 5 presents a meridional section of the mean zonal wind (contours) and the variability of the meridional wind (shading) for the ERA5 reanalysis and the coupled model. The winds were filtered over the 2–10 day band, as well as the 3–5 day and 6–9 day bands. The results were then zonally averaged between 25°W and 15°W for the JAS period over 2001–2021. Overall, the coupled model reproduces the atmospheric column winds quite satisfactorily, exhibiting a spatial structure similar to that of the ERA5 data. However, the model produces a stronger wind signal than ERA5, with differences around 1 m/s for the mean zonal wind and about 1.25 m/s for the standard deviation of the meridional wind. The African Easterly Jet is clearly distinguishable, with its core located near 600 hPa and 15°N, and wind

https://doi.org/10.5194/egusphere-2025-4429
Preprint. Discussion started: 26 September 2025

speeds of 12 m/s in ERA5 and 11 m/s in the coupled model. At the level of the African Easterly Jet, two maxima of meridional wind variability are observed: around 15°N for $AEWs_{3-5day}$ and around 25°N for $AEWs_{6-9day}$. A maximum of meridional wind variability at low altitude (around 900hPa) is also observed between 16°N and 18°N for $AEWs_{3-5day}$. These observations are similar to Wu et al. (2013) description of the two AEWs regimes. Around 10°N, the West African westerly jet is visible, with mean winds reaching 3 m/s for ERA5 and 4 m/s for the coupled model. It extends from the surface to 800hPa. This lower tropospheric dynamic is known to be the driver of moisture supply (coming from the ocean) to the West African rain system (Lamb, 1983; Grist and Nicholson, 2001; Liu et al., 2020).

Overall, this comparison between the coupled model and atmospheric and oceanic datasets provides strong confidence in the model's ability to represent the main characteristics of AEWs and SST variability. It also suggests that the 3–5 day band contains most of the energy near the surface and is therefore expected to have the greatest impact on SSTs.

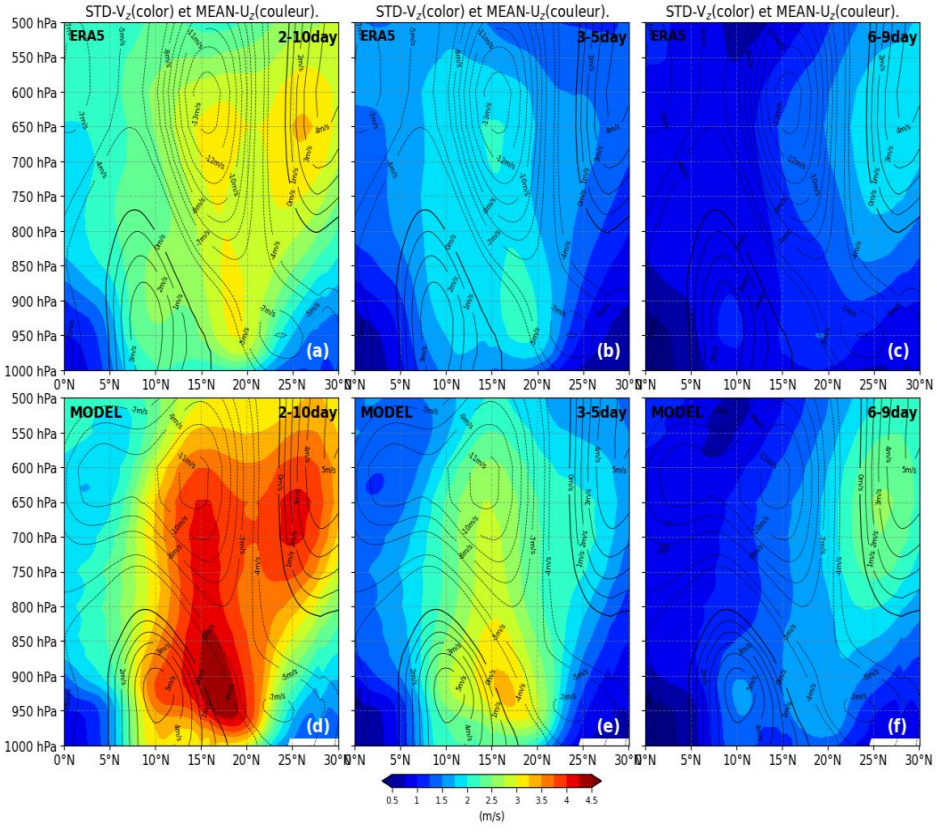

Figure 5: Latitudinal section of the standard deviation of meridional wind anomalies, longitudinally averaged between 25°W and 15°W, during JAS over the 2001–2021 period for (a), (b), (c) ERA5 and (d), (e), (f) the coupled model. Anomalies are band-pass filtered in the 2–10-day (left panels), 3–5-day (middle

https://doi.org/10.5194/egusphere-2025-4429
Preprint. Discussion started: 26 September 2025

panels), and 6–9-day (right panels) ranges. Mean zonal winds are shown as contours to highlight the zonal jets.

4 Ocean surface response to AEWs

4.1 An index representative of AEWs

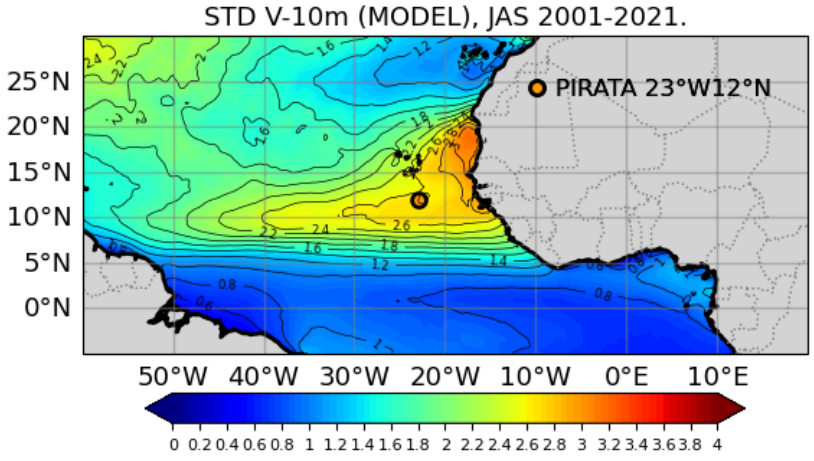

Figure 6: Standard deviation of the 10-m meridional wind anomalies (V-10m), band-pass filtered in the 2–10-day range, during the JAS period from 2001 to 2021 for the coupled model. The location of the PIRATA mooring at 23°W-12°N is indicated with a black circle. It lies within the area of maximum variability.

The colocalization of high wind and SST variability bands near 10°N (Fig. 1, Fig. 3), together with the peak variability observed during JAS for both variables, strongly suggest a link between AEWs and the high-frequency variability of SSTs. The influence of AEWs on the ocean surface of the North tropical Atlantic is assessed by projecting the anomalies of relevant physical fields onto an index designed to be representative of AEWs activity. In many previous studies, this index has been derived from the characteristic fields at the heart of these disturbances, such as meridional wind, relative vorticity, or outgoing longwave radiation (OLR), and has been applied to atmospheric variables (Diedhiou et al., 2001; Fink and Reiner, 2003; Jiang et al., 2023; Kiladis et al., 2006). Given our focus on the impact of AEWs on SST, and the distinctive surface signature of AEWs (Fig. 5), we have selected a 10-m surface wind index corresponding to the mean meridional wind filtered over the 2-10-day period. The reference point for this index is set at the PIRATA mooring located at 23°W -12°N—an area of strong variability, sufficiently offshore to avoid coastal effects (Figure 6). Note that various index locations have been tested, including the site at 17.5°W-15°N proposed by Kiladis et al. (2006), but the results showed similar patterns and only minor differences in amplitude (not shown).

https://doi.org/10.5194/egusphere-2025-4429
Preprint. Discussion started: 26 September 2025

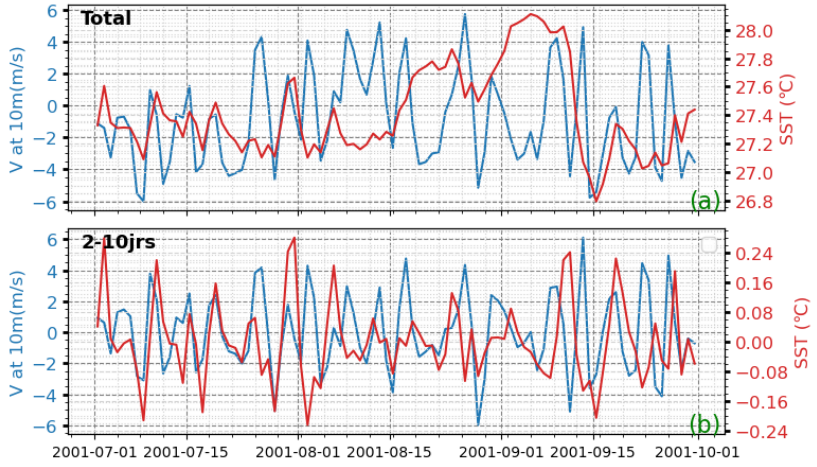

Figure 7: SST (in red) and 10-m meridional wind velocity (in blue) at 23°W-12°N during JAS 2015 for the coupled model: (a) non-filtered data, (b) band-pass filtered in the 2–10-day range.

To illustrate the relationship between SST and the 10-m meridional wind, Figure 7 shows their evolution during the boreal summer of 2015, along with the 2–10 day band-pass filtered anomalies. The 10-m meridional wind alternates between southward (negative) and northward (positive) directions, as the area is located within the ITCZ during this period, resulting in fluctuations ranging from -5 m/s to 5 m/s. The high-frequency peaks, although generally offset by about 1-2 days, show a notable degree of correspondence, particularly in July, when strong southward wind bursts are often associated with surface cooling (Fig. 7b).

4.2 Signature of AEWs on the SST

To investigate the impact of AEWs on SSTs, we performed a lagged linear regression analysis using different model variables and the AEWs index, as defined in Section 4.1. The following results are subject to a student's t-test, and only the statistically significant local fields (>95%) are shown. Figure 8 shows the regression of the meridional winds at different time lags (in days), displaying the evolution of patterns typical of AEWs. Southwest–northeast oriented structures, with a meridional extent of 25–30° (about 3,000 km) and a zonal extent of 15°, propagate from east to west. They originate from Central Africa with the lowest amplitude and spread towards West Africa. They reach a maximum amplitude (> 6 m/s) over the coastal regions at 15–20°N and then gradually dissipate as they propagate westward in the central basin. This spatial and temporal behavior closely resembles that of structures observed at higher altitudes (e.g., Hsieh and Cook, 2007; Thorncroft et al., 2008; Leroux and Hall, 2009).

https://doi.org/10.5194/egusphere-2025-4429
Preprint. Discussion started: 26 September 2025

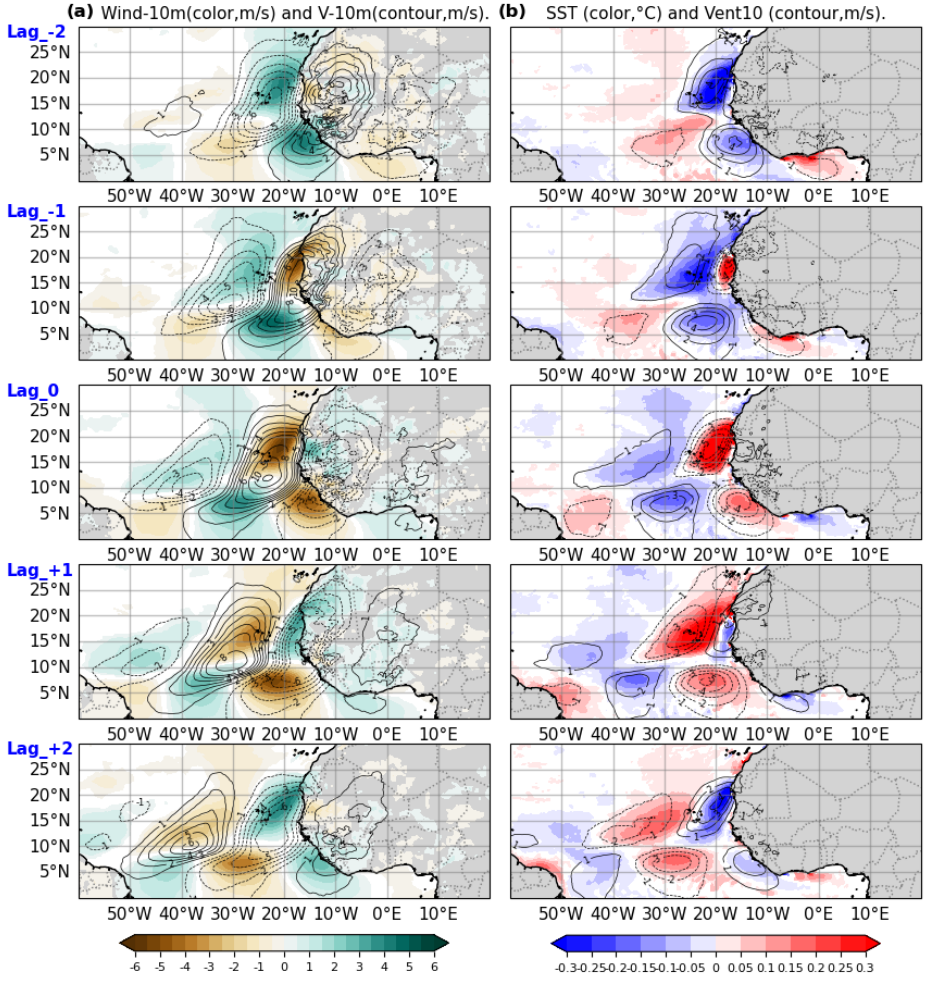

Figure 8: Lagged regression of atmospheric and oceanic variables onto the 2–10-day AEWs index, defined as the 10-m meridional wind anomaly at 23°W-12°N (with a positive index corresponding to a northward wind anomaly). Left panels show 10-m wind speed anomalies (shading) and meridional wind anomalies (contours). Right panels show SST anomalies (shading) and meridional wind anomalies (contours). Regressions are presented at different time lags (in days) to capture the temporal evolution associated with AEWs passage. The AEWs index time series used here is illustrated in Figure 7.

As they propagate westward, AEWs structures associated with 2–10-day 10-m meridional wind anomalies exert opposite effects on the total surface wind field on either side of the Intertropical Convergence Zone (ITCZ). Specifically, a positive meridional wind anomaly leads to a weakening of the total wind speed north of the ITCZ and a strengthening of the wind south of it (Fig. 8a). The SST anomalies regressed on the AEWs index exhibit cooling and warming patterns that propagate from east to west, with stronger winds generally associated with cool SST anomalies (± 0.5 °C), and weaker winds

https://doi.org/10.5194/egusphere-2025-4429
Preprint. Discussion started: 26 September 2025

with warm anomalies (Fig. 8b). The modulation of wind intensity contributes directly to the dipole pattern of SST variability, suggesting that AEWs play a significant role in modulating SSTs through surface winds.

5 The ocean mixed layer heat balance

To better characterize the mechanisms through which the AEWs modulate SST in the tropical North Atlantic, we analyze the heat budget of the oceanic mixed layer (Jouanno et al., 2011). This approach is particularly well-suited for isolating and quantifying the physical processes that drive temperature changes in the surface layer, including air-sea heat exchanges, horizontal advection, and vertical diffusion. The various terms of the heat budget were evaluated in the model, and the temperature evolution in the surface layer, for a layer of thickness h, can be expressed as follows:

$$\partial_t T = -\langle u\partial_x T\rangle_h - \langle v\partial_y T\rangle_h - \langle w\partial_z T\rangle_h + \langle D_t\rangle_h + \frac{(K_z\partial_z T)_{z=-h}}{h} + \frac{Q_s(1-F_{-h}) + Q_{ns}}{\rho_0 C_p h}$$

Here, T represents temperature; u, v, and w correspond to the zonal, meridional, and vertical currents, respectively. F_{-h} refers to the fraction of solar radiation reaching depth h in the surface layer. This depth is defined as 5 m to ensure that the integrated trends remain consistent with near-surface ocean conditions. This equation represents the temperature evolution as the sum of the tendency terms related to horizontal and vertical advection, lateral and vertical diffusion and the atmospheric component which represents the combined effects of the solar flux Q_s and the non-solar flux Q_{ns}. This latter includes net long-wave, sensible and latent heat fluxes. Terms related to oceanic processes (advection and diffusion) are grouped under T_OCEAN, while atmospheric terms are separated into non-solar surface fluxes (T_Q_{ns}) and solar fluxes (T_Q_s).

5.1 Oceanic processes versus heat fluxes in AEW-induced SST evolution

As with SST, the different terms were time-filtered within the 2–10 day range prior to performing the regressions. Regressions were computed for the JAS period at time lags ranging from two days prior to two days after the AEW index, enabling us to track the evolution of each term during an AEW passage. For comparison, lagged regressions of 10 m wind speed, outgoing longwave radiation (OLR) and mixed layer depth are also superimposed.

Figure 9 shows the regressions of the total temperature tendency and the different heat budget terms on the AEW index. As noted earlier, the impact of AEWs on SST is strongest in coastal regions, where their signature is most pronounced, and gradually weakens as they propagate offshore (Fig. 9a). At zero lag, the regression shows warming around 23°W–12°N, corresponding to a northward wind anomaly at the index location and a negative total wind speed anomaly. The evolution of SST associated with AEWs appears to result from multiple processes acting together. All of these processes contribute significantly to temperature changes, with none being negligible, and their effects are not perfectly in phase. Term

https://doi.org/10.5194/egusphere-2025-4429
Preprint. Discussion started: 26 September 2025

T_Q_{ns} (Fig. 9b) exhibits patterns resembling the overall temperature tendency but opposite to the wind anomalies, which can be explained by the fact that increased wind speed enhances latent heat flux (not shown), leading to SST cooling. Although weaker, solar radiation also contributes to the overall trend, which is linked to the modulation of cloud cover (OLR, contours in Fig. 9c). For example, a cooling rate of –0.2°C/day for (T_Q_s corresponds to an OLR minimum of –40 W/m², and vice versa. Interestingly, these contributions are out of phase with (T_Q_{ns}, with the largest effects occurring north of 10°N, near the ITCZ during JAS.

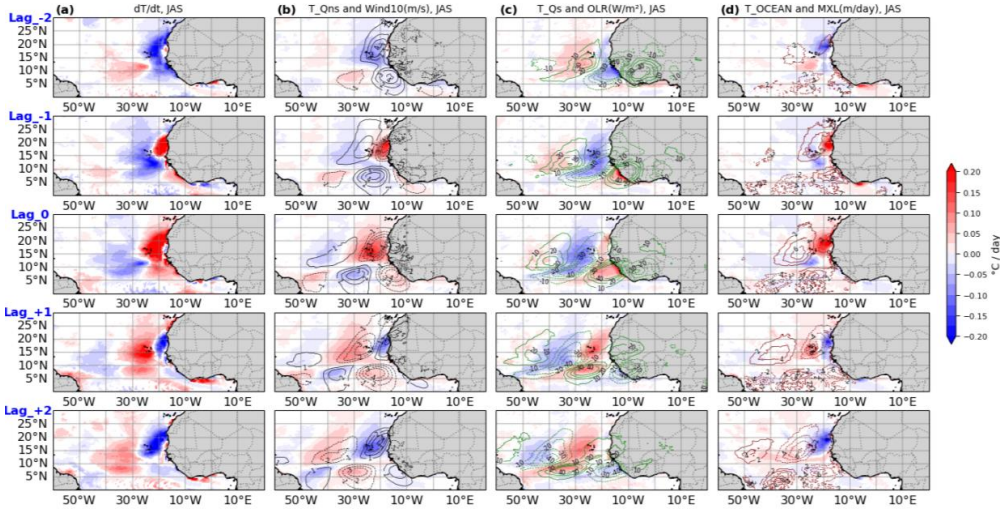

Figure 9: Lagged evolution of anomalies in the mixed-layer heat budget terms, regressed onto the 2–10-day AEWs index. Panels show: (column a) mixed-layer temperature tendency (dT/dt), (b) contribution from non-solar surface heat fluxes ((T_Q_{ns}, shading) with 10-m wind speed anomalies overlaid (contours), (c) contribution from solar radiation ((T_Q_s, shading) with OLR anomalies (contours), and (d) oceanic processes (T_OCEAN, shading) with mixed-layer depth (MXL) anomalies (contours). Regressions are presented at different time lags (in days) to capture the temporal evolution associated with AEWs passage.

The contribution of oceanic processes to SST modulation represents a key part of the ocean's response to AEWs (Fig. 9d). Note that thermal advection is negligible offshore and very weak near some coastal areas. Vertical mixing (vertical diffusion) primarily controls T_OCEAN (not shown). The observed cooling and warming patterns correspond, respectively, to positive (deepening) and negative (shallowing) mixed layer depth anomalies of approximately ±6 m. The temporal evolution at different lags reveals that the cooling induced by T_OCEAN is associated with increasing wind speeds (Fig. 9b), indicating that the two signals (wind and T_OCEAN) are in phase quadrature. This indicates that the intensified winds associated with AEWs deepen the mixed layer, entraining cooler subsurface water to the surface and thereby cooling the SST. At zero lag, T_Q_{ns} cooling rates reach approximately -0.2 °C/day, while the oceanic contribution (mainly vertical mixing) accounts for up to -0.15 °C/day,

https://doi.org/10.5194/egusphere-2025-4429
Preprint. Discussion started: 26 September 2025

confirming that both mechanisms contribute with comparable magnitudes. Thus, the SST response to AEWs results from a complex interplay between the effects of local wind speed on air-sea fluxes, the modulation of solar radiation by cloud cover, and the mixed layer deepening during phases of wind fluctuations.

5.2 Dissociating the impact of AEWs in the 3-5 and 6-9-day bands

As discussed previously, AEWs occur over two distinct time scales, typically corresponding to the 3–5-day and 6–9-day bands, which have different meridional distributions. Consequently, the regression results presented earlier may be biased toward the more dominant wave band. To determine whether similar processes occur for both wave types, we perform regression analyses of dT/dt and its contributing terms using indices filtered separately for each band (Figure 10). The results confirm that AEWs in the 3–5-day band have a significantly greater impact on SST compared to those in the 6–9-day band. This is consistent with the surface signature of $AEWs_{3-5day}$ between 5°N and 25°N, as opposed to the higher-altitude and more northerly $AEWs_{6-9day}$ structures (Fig. 5). For both types of AEWs, the results indicate that the SST response arises from a combination of air-sea fluxes and vertical mixing, contributing in roughly equal proportions.

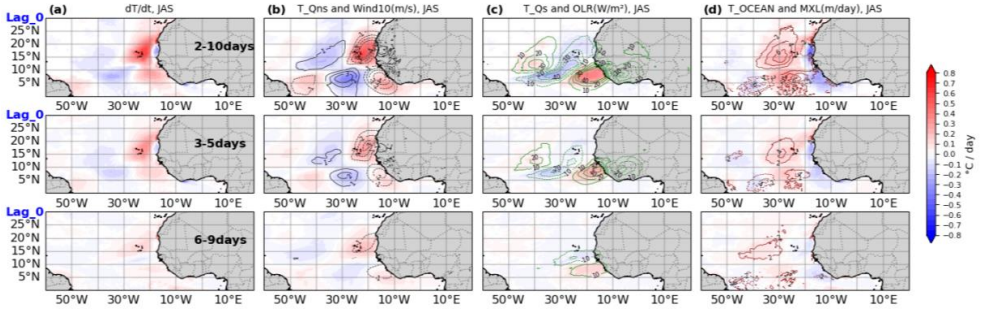

Figure 10: Same as Figure 9, but shown at lag 0 only. Panels present anomalies in the surface layer temperature tendency (dT/dt) and its contributing terms for the 2–10-day (top panels), 3–5-day (middle panels), and 6–9-day bands (bottom panels).

6 Conclusion

A 21-year regional coupled simulation over the tropical Atlantic is used to investigate the influence of African Easterly Waves on SST in the North Tropical Atlantic and to quantitatively assess the underlying processes. Although small biases in SST and wind are present, comparisons with reference satellite observations and atmospheric reanalysis datasets demonstrate that the simulation provides a robust framework and a solid tool for studying ocean–atmosphere interactions in the tropical Atlantic. The characteristics of AEWs—represented by westward-propagating meridional wind anomalies between 5°N and 25°N, with a typical zonal wavelength of about 15°—are well captured by the

https://doi.org/10.5194/egusphere-2025-4429
Preprint. Discussion started: 26 September 2025

simulation and show good agreement with observations and reanalysis datasets. In addition, the temporal separation into 3–5-day and 6–9-day variability reveals distinct branches characterized by their latitude and vertical structure, in agreement with the literature. This study highlights for the first time a consistent AEW-related imprint on SST in the tropical Atlantic, with anomalies occasionally exceeding ±0.5 °C. The combined effect of latent heat fluxes, shortwave radiation, and vertical mixing underscores the critical role of AEWs in shaping mixed-layer dynamics.

The signature of AEWs on SST is identified by projecting filtered wind anomalies — used as a representative AEW index — onto SST fields, revealing a significant and consistent AEW-related imprint. A similar projection applied to the temperature tendency terms of the heat budget shows that AEW-related SST anomalies result from a combination of non-solar heat flux fluctuations (mainly latent) driven by surface winds, shortwave radiation variations linked to cloud cover changes, and modulation of ocean mixing associated with mixed-layer variability. The results also highlight a stronger SST response between 5°N and 20°N from 3–5-day AEWs compared to 6–9-day AEWs, consistent with their more pronounced surface signal south of 20°–25°N. While such methodologies have been applied to atmospheric fields, to our knowledge, this is the first time that this type of identification has been demonstrated for oceanic fields.

This quantitative assessment of the impact of African Easterly Waves (AEWs) on dynamic and thermodynamic heat fluxes is useful when compared with previous studies. Several studies have shown that the role of atmospheric wind and latent heat fluxes dominates variability from intraseasonal to interdecadal timescales (Foltz et al., 2003), while the role of mixing has mainly been identified as enhancing in the upper thermocline within 2°N–2°S (Jouanno et al., 2011) relative to off-equatorial regions (Hummels et al., 2014). However, turbulence remains the most challenging component to quantify and assess, and high-frequency phenomena can also contribute to local mixing outside the equatorial region (Foltz et al., 2020; Hummels et al., 2020). The mixing component may reflect the influence of near-inertial currents, which align with the seasonal cycle of AEWs and enhance turbulent mixing over extensive regions of the eastern tropical North Atlantic (D'Asaro, 1985; Plueddemann and Farrar, 2006; Hummels et al., 2020). The next step is therefore to investigate the role of near-inertial activity in the mixing contribution, noting that the model's near-inertial kinetic energy levels are comparable in both spatial distribution and amplitude to previous estimates (not shown).

This raises questions about our methodology, which relies on regressing wind fields onto variables such as SST. While this approach primarily captures synchronous responses, it may overlook effects that occur out of phase. Tests applying time lags from –2 to +2 days did not significantly change the results. This indicates that, unlike the more immediate effects of solar radiation and latent heat fluxes linked to cloud cover and wind fluctuations, the influence of near-inertial waves—generated by AEW-related wind bursts and potentially propagating over several days—may be underestimated. The study highlights the need for additional numerical experiments, such as masking AEWs by nudging winds

https://doi.org/10.5194/egusphere-2025-4429
Preprint. Discussion started: 26 September 2025

toward climatology, to better isolate oceanic processes and their influence on interannual timescales. Beyond advancing process understanding, these findings are relevant for improving the representation of synoptic variability in coupled models, reducing persistent SST biases, and ultimately enhancing tropical cyclone prediction and seasonal climate forecasts.

https://doi.org/10.5194/egusphere-2025-4429
Preprint. Discussion started: 26 September 2025

Open research

Temperature, salinity, wind and heat flux data from the PIRATA moorings used in this study are available from the Global Tropical Moored Buoy Array at https://www.pmel.noaa.gov/tao/drupal/disdel/. NOAA OI SST V2 High Resolution Dataset data provided by the NOAA PSL, Boulder, Colorado, USA (https://doi.org/10.1175/JCLI-D-20-0166.1). ERA5, ASCAT. Numerical simulated fields used for diagnostics are available at (https://doi.org/10.6084/m9.figshare.30095101). All analyses were performed and all figures created using Python.

Author contributions

MM: Investigation, Software, Visualization, Writing (original draft), Review and Editing (original draft).
FG: Project administration, Supervision, Validation, Writing (original draft), Review and Editing (original draft).
MG: Software, Validation, Writing (original draft), Review and Editing (original draft).
MD: Review and Editing (original draft).
IS: Review and Editing (original draft).
JJ: Supervision, Validation, Writing (original draft), Review and Editing (original draft).

Acknowledgments

This work was supported by the French National program CNES TOSCA NICITA project. M.M. is funded by the French National Research Institute for Sustainable Development (IRD) through an ARTS grant. Computing resources were provided by DARI under grant GEN7298. The authors also acknowledge the GTMBA Project Office of NOAA/PMEL and the PIRATA program for freely providing data from the tropical Atlantic buoy array.

https://doi.org/10.5194/egusphere-2025-4429
Preprint. Discussion started: 26 September 2025

References

Banzon, V., Smith, T. M., Chin, T. M., Liu, C., and Hankins, W.: A long-term record of blended satellite and in situ sea-surface temperature for climate monitoring, modeling and environmental studies, Earth System Science Data, 8, 165–176, https://doi.org/10.5194/essd-8-165-2016, 2016.

Bercos-Hickey, E. and Patricola, C. M.: Drivers of Atlantic Tropical Cyclogenesis: African Easterly Waves and the Environment, Geophysical Research Letters, 52, e2024GL112002, https://doi.org/10.1029/2024GL112002, 2025.

Bercos-Hickey, E., Nathan, T. R., and Chen, S.-H.: Saharan dust and the African easterly jet–African easterly wave system: Structure, location and energetics, Quarterly Journal of the Royal Meteorological Society, 143, 2797–2808, https://doi.org/10.1002/qj.3128, 2017.

Berry, G. J. and Thorncroft, C.: Case Study of an Intense African Easterly Wave, Monthly Weather Review, 133, 752–766, https://doi.org/10.1175/MWR2884.1, 2005.

Bourlès, B., Lumpkin, R., McPhaden, M. J., Hernandez, F., Nobre, P., Campos, E., Yu, L., Planton, S., Busalacchi, A., Moura, A. D., Servain, J., and Trotte, J.: THE PIRATA PROGRAM: History, Accomplishments, and Future Directions*, Bulletin of the American Meteorological Society, 89, 1111–1126, https://doi.org/10.1175/2008BAMS2462.1, 2008.

Burpee, R. W.: The Origin and Structure of Easterly Waves in the Lower Troposphere of North Africa, 1972.

Carlson, T. N.: SOME REMARKS ON AFRICAN DISTURBANCES AND THEIR PROGRESS OVER THE TROPICAL ATLANTIC, 1969.

Craig, A., Valcke, S., and Coquart, L.: Development and performance of a new version of the OASIS coupler, OASIS3-MCT_3.0, Geoscientific Model Development, 10, 3297–3308, https://doi.org/10.5194/gmd-10-3297-2017, 2017.

Cromwell, T.: Circulation in a meridional plane in the central equatorial Pacific, 1953.

Danso, D. K., Patricola, C. M., and Bercos-Hickey, E.: Influence of African Easterly Wave Suppression on Atlantic Tropical Cyclone Activity in a Convection-Permitting Model, Geophysical Research Letters, 49, e2022GL100590, https://doi.org/10.1029/2022GL100590, 2022.

D'Asaro, E. A.: The energy flux from the wind to near-inertial motions in the surface mixed layer, Journal of Physical Oceanography, 15, 1043–1059, 1985.

https://doi.org/10.5194/egusphere-2025-4429
Preprint. Discussion started: 26 September 2025

Deppenmeier, A.-L., Haarsma, R. J., Heerwaarden, C. van, and Hazeleger, W.: The Southeastern Tropical Atlantic SST Bias Investigated with a Coupled Atmosphere–Ocean Single-Column Model at a PIRATA Mooring Site, Journal of Climate, 33, 6255–6271, https://doi.org/10.1175/JCLI-D-19-0608.1, 2020.

Diedhiou, A., Janicot, S., Viltard, A., De Felice, P., and Laurent, H.: A fast moving easterly wave of the West Africa troposphere, Meteorology and Atmospheric Physics, 69, 39–47, 1998a.

Diedhiou, A., Janicot, S., Viltard, A., and de Felice, P.: Evidence of two regimes of easterly waves over West Africa and the tropical Atlantic, Geophysical Research Letters, 25, 2805–2808, 1998b.

Diedhiou, A., Janicot, S., Viltard, A., de Felice, P., and Laurent, H.: Easterly wave regimes and associated convection over West Africa and tropical Atlantic: results from the NCEP/NCAR and ECMWF reanalyses, Climate Dynamics, 15, 795–822, https://doi.org/10.1007/s003820050316, 1999.

Diedhiou, A., Janicot, S., Viltard, A., and de Félice, P.: Composite patterns of easterly disturbances over West Africa and the tropical Atlantic: a climatology from the 1979–95 NCEP/NCAR reanalyses, Climate Dynamics, 18, 241–253, https://doi.org/10.1007/s003820100173, 2001.

Diedhiou, A., Machado, L. A. T., and Laurent, H.: Mean kinematic characteristics of synoptic easterly disturbances over the Atlantic, Adv. Atmos. Sci., 27, 483–499, https://doi.org/10.1007/s00376-009-9092-5, 2010.

Donlon, C. J., Minnett, P. J., Gentemann, C., Nightingale, T. J., Barton, I. J., Ward, B., and Murray, M. J.: Toward Improved Validation of Satellite Sea Surface Skin Temperature Measurements for Climate Research, Journal of Climate, 15, 353–369, https://doi.org/10.1175/1520-0442(2002)015%253C0353:TIVOSS%253E2.0.CO;2, 2002.

Dunkerton, T. J., Montgomery, M., and Wang, Z.: Tropical cyclogenesis in a tropical wave critical layer: Easterly waves, Atmospheric Chemistry and Physics, 9, 5587–5646, 2009.

Dutton, J. A.: Dynamics of atmospheric motion, (No Title), 1986.

Emanuel, K.: Increasing destructiveness of tropical cyclones over the past 30 years, Nature, 436, 686–688, https://doi.org/10.1038/nature03906, 2005.

Enfield, D. B. and Lee, S.: The Heat Balance of the Western Hemisphere Warm Pool, Journal of Climate, 18, 2662–2681, https://doi.org/10.1175/JCLI3427.1, 2005.

https://doi.org/10.5194/egusphere-2025-4429
Preprint. Discussion started: 26 September 2025

Felice, P. D., Monkam, D., Viltard, A., and Ouss, C.: Characteristics of North African 6–9 Day Waves during Summer 1981, Monthly Weather Review, 118, 2624–2633, https://doi.org/10.1175/1520-0493(1990)118%253C2624:CONADW%253E2.0.CO;2, 1990.

Felice, P. de, Viltard, A., and Oubuih, J.: A Synoptic-Scale Wave of 6–9-Day Period in the Atlantic Tropical Troposphere during Summer 1981, Monthly Weather Review, 121, 1291–1298, https://doi.org/10.1175/1520-0493(1993)121%253C1291:ASSWOD%253E2.0.CO;2, 1993.

Ferry, N., Parent, L., Garric, G., Bricaud, C., Testut, C., Le Galloudec, O., Lellouche, J., Drevillon, M., Greiner, E., and Barnier, B.: GLORYS2V1 global ocean reanalysis of the altimetric era (1992–2009) at meso scale, Mercator Ocean–Quaterly Newsletter, 44, 2012.

Fink, A. H. and Reiner, A.: Spatio-temporal variability of the relation between African easterly waves and West African squall lines in 1998 and 1999., , 108, 2003.

Fleagle, R. G. and Businger, J. A.: An introduction to atmospheric physics, Academic Press, 1981.

Foltz, G. R., Grodsky, S. A., Carton, J. A., and McPhaden, M. J.: Seasonal mixed layer heat budget of the tropical Atlantic Ocean, Journal of Geophysical Research: Oceans, 108, https://doi.org/10.1029/2002JC001584, 2003.

Foltz, G. R., Hummels, R., Dengler, M., Perez, R. C., and Araujo, M.: Vertical Turbulent Cooling of the Mixed Layer in the Atlantic ITCZ and Trade Wind Regions, Journal of Geophysical Research: Oceans, 125, e2019JC015529, https://doi.org/10.1029/2019JC015529, 2020.

Garnesson, P., Mangin, A., Fanton d'Andon, O., Demaria, J., and Bretagnon, M.: The CMEMS GlobColour chlorophyll a product based on satellite observation: multi-sensor merging and flagging strategies, Ocean Science, 15, 819–830, https://doi.org/10.5194/os-15-819-2019, 2019.

Gévaudan, M., Jouanno, J., Durand, F., Morvan, G., Renault, L., and Samson, G.: Influence of ocean salinity stratification on the tropical Atlantic Ocean surface, Clim Dyn, 57, 321–340, https://doi.org/10.1007/s00382-021-05713-z, 2021.

Gévaudan, M., Durand, F., and Jouanno, J.: Influence of the Amazon-Orinoco Discharge Interannual Variability on the Western Tropical Atlantic Salinity and Temperature, Journal of Geophysical Research: Oceans, 127, e2022JC018495, https://doi.org/10.1029/2022JC018495, 2022.

Gill, A. E.: Some simple solutions for heat-induced tropical circulation, Quarterly Journal of the Royal Meteorological Society, 106, 447–462, https://doi.org/10.1002/qj.49710644905, 1980.

https://doi.org/10.5194/egusphere-2025-4429
Preprint. Discussion started: 26 September 2025

Graham, N. E. and Barnett, T. P.: Sea Surface Temperature, Surface Wind Divergence, and Convection over Tropical Oceans, Science, 238, 657–659, https://doi.org/10.1126/science.238.4827.657, 1987.

Grist, J. P.: Easterly Waves over Africa. Part I: The Seasonal Cycle and Contrasts between Wet and Dry Years, Monthly Weather Review, 130, 197–211, https://doi.org/10.1175/1520-0493(2002)130%253C0197:EWOAPI%253E2.0.CO;2, 2002.

Grist, J. P. and Nicholson, S. E.: A Study of the Dynamic Factors Influencing the Rainfall Variability in the West African Sahel, Journal of Climate, 14, 1337–1359, https://doi.org/10.1175/1520-0442(2001)014%253C1337:ASOTDF%253E2.0.CO;2, 2001.

Hastenrath, S. and Greischar, L.: Circulation mechanisms related to northeast Brazil rainfall anomalies, Journal of Geophysical Research: Atmospheres, 98, 5093–5102, https://doi.org/10.1029/92JD02646, 1993.

Hersbach, H., Bell, B., Berrisford, P., Hirahara, S., Horányi, A., Muñoz-Sabater, J., Nicolas, J., Peubey, C., Radu, R., and Schepers, D.: The ERA5 global reanalysis, Quarterly Journal of the Royal Meteorological Society, 146, 1999–2049, 2020.

Hsieh, J.-S. and Cook, K. H.: A Study of the Energetics of African Easterly Waves Using a Regional Climate Model, Journal of the Atmospheric Sciences, 64, 421–440, https://doi.org/10.1175/JAS3851.1, 2007.

Huang, B., Liu, C., Freeman, E., Graham, G., Smith, T., and Zhang, H.-M.: Assessment and Intercomparison of NOAA Daily Optimum Interpolation Sea Surface Temperature (DOISST) Version 2.1, Journal of Climate, 34, 7421–7441, https://doi.org/10.1175/JCLI-D-21-0001.1, 2021.

Hummels, R., Dengler, M., Brandt, P., and Schlundt, M.: Diapycnal heat flux and mixed layer heat budget within the Atlantic Cold Tongue, Climate Dynamics, 43, 3179–3199, https://doi.org/10.1007/s00382-014-2339-6, 2014.

Hummels, R., Dengler, M., Rath, W., Foltz, G. R., Schütte, F., Fischer, T., and Brandt, P.: Surface cooling caused by rare but intense near-inertial wave induced mixing in the tropical Atlantic, Nature Communications, 11, 3829, https://doi.org/10.1038/s41467-020-17601-x, 2020.

J. Figa-Saldaña, M. R. D., J. J. W. Wilson, E. Attema, R. Gelsthorpe and Stoffelen, A.: The advanced scatterometer (ASCAT) on the meteorological operational (MetOp) platform: A follow on for European wind scatterometers, Canadian Journal of Remote Sensing, 28, 404–412, https://doi.org/10.5589/m02-035, 2002.

https://doi.org/10.5194/egusphere-2025-4429
Preprint. Discussion started: 26 September 2025

584 Janiga, M. A. and Thorncroft, C. D.: Regional differences in the kinematic and thermodynamic structure
585 of African easterly waves, Quarterly Journal of the Royal Meteorological Society, 139, 1598–1614,
586 https://doi.org/10.1002/qj.2047, 2013.

587 Jiang, X., Su, H., Chen, S. S., and Ullrich, P. A.: Simulation of African Easterly Waves in a Global
588 Climate Model, Journal of Climate, 36, 1415–1433, https://doi.org/10.1175/JCLI-D-22-0090.1, 2023.

589 Jonville, T., Flamant, C., and Lavaysse, C.: Dynamical study of three African easterly waves in
590 September 2021, Quarterly Journal of the Royal Meteorological Society, 150, 2489–2509, 2024.

591 Jonville, T., Cornillault, E., Lavaysse, C., Peyrillé, P., and Flamant, C.: Distinguishing north and south
592 African Easterly Waves with a spectral method: Implication for tropical cyclogenesis from mergers in
593 the North Atlantic, Quarterly Journal of the Royal Meteorological Society, 151, e4909,
594 https://doi.org/10.1002/qj.4909, 2025.

595 Jouanno, J., Marin, F., du Penhoat, Y., Sheinbaum, J., and Molines, J.-M.: Seasonal heat balance in the
596 upper 100 m of the equatorial Atlantic Ocean, Journal of Geophysical Research: Oceans, 116,
597 https://doi.org/10.1029/2010JC006912, 2011.

598 Kiladis, G. N., Thorncroft, C. D., and Hall, N. M. J.: Three-Dimensional Structure and Dynamics of
599 African Easterly Waves. Part I: Observations, Journal of the Atmospheric Sciences, 63, 2212–2230,
600 https://doi.org/10.1175/JAS3741.1, 2006.

601 Lamb, P. J.: Sub-saharan rainfall update for 1982; continued drought, Journal of climatology, 3, 419–
602 422, 1983.

603 Leroux, S. and Hall, N. M. J.: On the Relationship between African Easterly Waves and the African
604 Easterly Jet, Journal of the Atmospheric Sciences, 66, 2303–2316,
605 https://doi.org/10.1175/2009JAS2988.1, 2009.

606 Liu, W., Cook, K. H., and Vizy, E. K.: Role of the West African westerly jet in the seasonal and diurnal
607 cycles of precipitation over West Africa, Climate Dynamics, 54, 843–861,
608 https://doi.org/10.1007/s00382-019-05035-1, 2020.

609 Madec, G., Bell, M., Blaker, A., Bricaud, C., Bruciaferri, D., Castrillo, M., Calvert, D., Chanut, J.,
610 Clementi, E., Coward, A., Epicoco, I., Éthé, C., Ganderton, J., Harle, J., Hutchinson, K., Iovino, D., Lea,
611 D., Lovato, T., Martin, M., Martin, N., Mele, F., Martins, D., Masson, S., Mathiot, P., Mele, F.,
612 Mocavero, S., Müller, S., Nurser, A. J. G., Paronuzzi, S., Peltier, M., Person, R., Rousset, C., Rynders,
613 S., Samson, G., Téchené, S., Vancoppenolle, M., and Wilson, C.: NEMO Ocean Engine Reference
614 Manual, , https://doi.org/10.5281/zenodo.8167700, 2023.

https://doi.org/10.5194/egusphere-2025-4429
Preprint. Discussion started: 26 September 2025

Maritorena, S., d'Andon, O. H. F., Mangin, A., and Siegel, D. A.: Merged satellite ocean color data products using a bio-optical model: Characteristics, benefits and issues, Remote Sensing of Environment, 114, 1791–1804, https://doi.org/10.1016/j.rse.2010.04.002, 2010.

Mekonnen, A., Thorncroft, C. D., and Aiyyer, A. R.: Analysis of Convection and Its Association with African Easterly Waves, Journal of Climate, 19, 5405–5421, https://doi.org/10.1175/JCLI3920.1, 2006.

Mickett, J. B., Serra, Y. L., Cronin, M. F., and Alford, M. H.: Resonant Forcing of Mixed Layer Inertial Motions by Atmospheric Easterly Waves in the Northeast Tropical Pacific, Journal of Physical Oceanography, 40, 401–416, https://doi.org/10.1175/2009JPO4276.1, 2010.

Moura, A. D. and Shukla, J.: On the Dynamics of Droughts in Northeast Brazil: Observations, Theory and Numerical Experiments with a General Circulation Model, Journal of Atmospheric Sciences, 38, 2653–2675, https://doi.org/10.1175/1520-0469(1981)038%253C2653:OTDODI%253E2.0.CO;2, 1981.

Murray, M. J., Allen, M. R., Merchant, C. J., Harris, A. R., and Donlon, C. J.: Direct observations of skin-bulk SST variability, Geophysical Research Letters, 27, 1171–1174, https://doi.org/10.1029/1999GL011133, 2000.

Nicholson, S. E.: A revised picture of the structure of the "monsoon" and land ITCZ over West Africa, Climate Dynamics, 32, 1155–1171, https://doi.org/10.1007/s00382-008-0514-3, 2009.

Nobre, P. and Shukla, J.: Variations of Sea Surface Temperature, Wind Stress, and Rainfall over the Tropical Atlantic and South America, Journal of Climate, 9, 2464–2479, https://doi.org/10.1175/1520-0442(1996)009%253C2464:VOSSTW%253E2.0.CO;2, 1996.

Opoku-Ankomah, Y. and Cordery, I.: Atlantic Sea Surface Temperatures and Rainfall Variability in Ghana, Journal of Climate, 7, 551–558, https://doi.org/10.1175/1520-0442(1994)007%253C0551:ASSTAR%253E2.0.CO;2, 1994.

Plueddemann, A. J. and Farrar, J. T.: Observations and models of the energy flux from the wind to mixed-layer inertial currents, Deep Sea Research Part II: Topical Studies in Oceanography, 53, 5–30, https://doi.org/10.1016/j.dsr2.2005.10.017, 2006.

Raj, J., Bangalath, H. K., and Stenchikov, G.: Future projection of the African easterly waves in a high-resolution atmospheric general circulation model, Climate Dynamics, 61, 3081–3102, https://doi.org/10.1007/s00382-023-06720-y, 2023.

https://doi.org/10.5194/egusphere-2025-4429
Preprint. Discussion started: 26 September 2025

Reed, R. J., Klinker, E., and Hollingsworth, A.: The structure and characteristics of African easterly wave disturbances as determined from the ECMWF operational analysis/forecast system, Meteorology and Atmospheric Physics, 38, 22–33, https://doi.org/10.1007/BF01029944, 1988.

Reynolds, R. W., Smith, T. M., Liu, C., Chelton, D. B., Casey, K. S., and Schlax, M. G.: Daily High-Resolution-Blended Analyses for Sea Surface Temperature, Journal of Climate, 20, 5473–5496, https://doi.org/10.1175/2007JCLI1824.1, 2007.

Richter, I. and Tokinaga, H.: An overview of the performance of CMIP6 models in the tropical Atlantic: mean state, variability, and remote impacts, Climate Dynamics, 55, 2579–2601, https://doi.org/10.1007/s00382-020-05409-w, 2020.

Russell, J. O., Aiyyer, A., White, J. D., and Hannah, W.: Revisiting the connection between African Easterly Waves and Atlantic tropical cyclogenesis, Geophysical Research Letters, 44, 587–595, https://doi.org/10.1002/2016GL071236, 2017.

Russell, J. O. H., Aiyyer, A., and Dylan White, J.: African Easterly Wave Dynamics in Convection-Permitting Simulations: Rotational Stratiform Instability as a Conceptual Model, Journal of Advances in Modeling Earth Systems, 12, e2019MS001706, https://doi.org/10.1029/2019MS001706, 2020.

Semunegus, H., Mekonnen, A., and Schreck III, C. J.: Characterization of convective systems and their association with African easterly waves, International Journal of Climatology, 37, 4486–4492, https://doi.org/10.1002/joc.5085, 2017.

Shi, Y., Huang, W., Wang, B., Yang, Z., He, X., and Qiu, T.: Origin of Warm SST Bias over the Atlantic Cold Tongue in the Coupled Climate Model FGOALS-g2, Atmosphere, 9, https://doi.org/10.3390/atmos9070275, 2018.

Skamarock, C., Klemp, B., Dudhia, J., Gill, O., Liu, Z., Berner, J., Wang, W., Powers, G., Duda, G., Barker, D. M., and Huang, X.: A Description of the Advanced Research WRF Model Version 4, 2019.

Skinner, C. B. and Diffenbaugh, N. S.: The contribution of African easterly waves to monsoon precipitation in the CMIP3 ensemble, Journal of Geophysical Research: Atmospheres, 118, 3590–3609, 2013.

Stommel, H.: Wind-drift near the equator, Deep Sea Research (1953), 6, 298–302, https://doi.org/10.1016/0146-6313(59)90088-7, 1959.

Sultan, B. and Janicot, S.: Abrupt shift of the ITCZ over West Africa and intra-seasonal variability, Geophysical Research Letters, 27, 3353–3356, https://doi.org/10.1029/1999GL011285, 2000.

https://doi.org/10.5194/egusphere-2025-4429
Preprint. Discussion started: 26 September 2025

674 Sweet, W., Fett, R., Kerling, J., and Violette, P. L.: Air-Sea Interaction Effects in the Lower Troposphere
675 Across the North Wall of the Gulf Stream, Monthly Weather Review, 109, 1042–1052,
676 https://doi.org/10.1175/1520-0493(1981)109%253C1042:ASIEIT%253E2.0.CO;2, 1981.

677 Thompson, R. M., Payne, S. W., Recker, E. E., and Reed, R. J.: Structure and Properties of Synoptic-
678 Scale Wave Disturbances in the Intertropical Convergence Zone of the Eastern Atlantic, 1979.

679 Thorncroft, C. and Hodges, K.: African Easterly Wave Variability and Its Relationship to Atlantic
680 Tropical Cyclone Activity, Journal of Climate, 14, 1166–1179, https://doi.org/10.1175/1520-
681 0442(2001)014%253C1166:AEWVAI%253E2.0.CO;2, 2001.

682 Thorncroft, C. D., Hall, N. M. J., and Kiladis, G. N.: Three-Dimensional Structure and Dynamics of
683 African Easterly Waves. Part III: Genesis, Journal of the Atmospheric Sciences, 65, 3596–3607,
684 https://doi.org/10.1175/2008JAS2575.1, 2008.

685 Tomaziello, A. C. N., Carvalho, L. M. V., and Gandu, A. W.: Intraseasonal variability of the Atlantic
686 Intertropical Convergence Zone during austral summer and winter, Climate Dynamics, 47, 1717–1733,
687 https://doi.org/10.1007/s00382-015-2929-y, 2016.

688 Valcke, S. and Redler, R.: The OASIS Coupler, in: Earth System Modelling - Volume 3: Coupling
689 Software and Strategies, edited by: Valcke, S., Redler, R., and Budich, R., Springer Berlin Heidelberg,
690 Berlin, Heidelberg, 23–32, https://doi.org/10.1007/978-3-642-23360-9_4, 2012.

691 Viltard, A., de Felice, P., and Oubuih, J.: Comparison of the African and the 6–9 day wave-like
692 disturbance patterns over West-Africa and the tropical Atlantic during summer 1985, Meteorology and
693 Atmospheric Physics, 62, 91–99, https://doi.org/10.1007/BF01037482, 1997.

694 Voldoire, A., Exarchou, E., Sanchez-Gomez, E., Demissie, T., Deppenmeier, A.-L., Frauen, C.,
695 Goubanova, K., Hazeleger, W., Keenlyside, N., and Koseki, S.: Role of wind stress in driving SST
696 biases in the Tropical Atlantic, Climate Dynamics, 53, 3481–3504, 2019.

697 Wade, M., Caniaux, G., and Du Penhoat, Y.: Variability of the mixed layer heat budget in the eastern
698 equatorial Atlantic during 2005–2007 as inferred using Argo floats, Journal of Geophysical Research:
699 Oceans, 116, 2011.

700 Waliser, D. E. and Graham, N. E.: Convective cloud systems and warm-pool sea surface temperatures:
701 Coupled interactions and self-regulation, Journal of Geophysical Research: Atmospheres, 98, 12881–
702 12893, https://doi.org/10.1029/93JD00872, 1993.

https://doi.org/10.5194/egusphere-2025-4429
Preprint. Discussion started: 26 September 2025

Wallace, J. M., Mitchell, T. P., and Deser, C.: The Influence of Sea-Surface Temperature on Surface Wind in the Eastern Equatorial Pacific: Seasonal and Interannual Variability, Journal of Climate, 2, 1492–1499, https://doi.org/10.1175/1520-0442(1989)002%253C1492:TIOSST%253E2.0.CO;2, 1989.

Wane, D., Lazar, A., Wade, M., and Gaye, A. T.: A Climatological Study of the Mechanisms Controlling the Seasonal Meridional Migration of the Atlantic Warm Pool in an OGCM, Atmosphere, 12, https://doi.org/10.3390/atmos12091224, 2021.

Wang, C., Enfield, D. B., Lee, S., and Landsea, C. W.: Influences of the Atlantic Warm Pool on Western Hemisphere Summer Rainfall and Atlantic Hurricanes, Journal of Climate, 19, 3011–3028, https://doi.org/10.1175/JCLI3770.1, 2006.

Wang, C., Lee, S.-K., and Enfield, D. B.: Atlantic Warm Pool acting as a link between Atlantic Multidecadal Oscillation and Atlantic tropical cyclone activity, Geochemistry, Geophysics, Geosystems, 9, https://doi.org/10.1029/2007GC001809, 2008.

Webster, P. J., Holland, G. J., Curry, J. A., and Chang, H.-R.: Changes in Tropical Cyclone Number, Duration, and Intensity in a Warming Environment, Science, 309, 1844–1846, https://doi.org/10.1126/science.1116448, 2005.

Wheeler, M. and Kiladis, G. N.: Convectively Coupled Equatorial Waves: Analysis of Clouds and Temperature in the Wavenumber–Frequency Domain, Journal of the Atmospheric Sciences, 56, 374–399, https://doi.org/10.1175/1520-0469(1999)056%253C0374:CCEWAO%253E2.0.CO;2, 1999.

Wu, M.-L. C., Reale, O., and Schubert, S. D.: A Characterization of African Easterly Waves on 2.5–6-Day and 6–9-Day Time Scales, Journal of Climate, 26, 6750–6774, https://doi.org/10.1175/JCLI-D-12-00336.1, 2013.